第 29 卷第 9 期
2013 年 9 月

无 机 化 学 学 报
CHINESE JOURNAL OF INORGANIC CHEMISTRY

Vol.29 No.9
1777-1786

键阻断原理构建中孔 A 型沸石

王 鹏 薛招腾 马静红* 亢玉红 李瑞丰*
(太原理工大学煤科学与技术教育部重点实验室,化学化工学院,精细化工研究所,太原 030024)

摘要: 采用不同类型的有机硅烷化 SiO_2 作为基本合成单元,制备了具有晶内中孔的 A 型沸石。考察了反应碱度、Si/Al 比、晶化时间等合成条件对产品的影响。结果表明,苯胺基丙基三甲氧基硅烷是合成中孔 A 型沸石的最佳硅烷化试剂;硅烷化试剂的应用,使中孔沸石晶化过程可以通过"键阻断原理"有效控制;沸石的中孔尺寸可以通过不同类型的有机硅烷化试剂进行调控; 一定范围内,其外比表面积、中孔体积随 SiO_2 表面硅烷化度的增加而增加。通过沸石晶化过程中的"键阻断",可以制备具有晶内中孔的 A 型沸石。

关键词: 催化; 键阻断; A 型沸石; 晶内中孔; 有机硅烷化
中图分类号: O611.4; O643.3; TQ426.6 **文献标识码**: A **文章编号**: 1001-4861(2013)09-1777-10
DOI:10.3969/j.issn.1001-4861.2013.00.269

Zeolite LTA with Intracrystal Mesopores Constructed by Bond-Blocking Principle

WANG Peng XUE Zhao-Teng MA Jing-Hong* KANG Yu-Hong LI Rui-Feng*
(*Key Laboratory of Coal Science and Technology, Ministry of Education, School of Chemistry and Chemical Engineering, Institute of Special Chemicals, Taiyuan University of Technology, Taiyuan* 030024, *China*)

Abstract: Zeolite LTA with intracrystal mesopores was built using four different organic functionized SiO_2 as configuration units. The effects of the synthesis conditions, including that of the alkalinity, the Si/Al molar ratio of synthesis mixture and crystallization time, on the growth process of the mesostructured zeolite crystals were investigated. Phenylaminopropyl-trimethoxysilane is the best candidate to create intracrystal mesopores in zeolite LTA crystals. The growth process of the mesostructured zeolite crystals was studied. Mesoporous size of the zeolite LTA can be modulated by selecting different kinds of organosilanes. Within a certain range, the external surface area and the mesoporous volume increase with the increasing organic function degree of the silica source. The results confirm that the synthesis method by the bond-blocking principle is an effective route to prepare zeolite LTA with tunable intracrystalline mesopores.

Key words: catalysis; bond-blocking principle; zeolite LTA; intracrystalline mesopores; organosilane; functionized SiO_2

0 Introduction

Zeolites are microporous aluminosilicate extensively used in the separation, purification and catalysis fields. They exhibit unique properties in above processes owing to the uniform, small pore size, the high surface area, a wide variety of exchangeable cations, the flexible frameworks, and the controlled chemical properties[1-8]. However, the major shortcoming of zeolites is that intrinsic micropore sizes impose not only a serious diffusion limit, but also a high backpressure on the flow system, restricting their

收稿日期:2013-03-22。收修改稿日期:2013-04-21。
国家自然科学基金(No.50872087)资助项目。
*通讯联系人。E-mail:rfli@tyut.edu.cn,majinghong@tyut.edu.cn

practical applications in relevant chemical industry[2-5].

To improve the diffusion property of large molecules in zeolites, in the past decades, various attempts have been made to modify the intrinsic structure of zeolites by introducing mesoporous structure, for example, via steaming, acid leaching, base leaching or chemical treatment[9-14]; the synthesis of nanosized zeolite with interparticle mesopores[15-18]; using mesoporous templates during synthesis, for example carbon black[19], carbon nanotubes[20], nanosized $CaCO_3$[21], aerogel[22]. With the aid of amphiphilic organosilane, Ryoo et al.[23-24] synthesized zeolite LTA and MFI with tunable mesoporosity. After that, a lot of research efforts were devoted to using organosilane as the mesoporous structure directing agent in zeolite synthesis.

Recently, we have demonstrated a synthesis method using organosilane to create intracrystal mesopores in conventional zeolite LTA and ZSM-5 by bond blocking effects[25-27]. The key of the method is the blocking actions of Si-C covalent bonds on the microcrystal surface during the growth process of crystals. During the organic functionalization of fumed silica, the hydrophilic moiety of the organosilane is hydrolyzed into hydroxyl, which can undergo a condensation or dehydration with the hydroxyl on the surface of fumed silica. Thus, the hydrophobic moiety of organosilane links the surface of fumed silica through Si-C covalent bond, which is stable enough under synthesis conditions[28-29]. During the synthesis process, the fumed silica enters into the framework of zeolite through covalent bonds of Si-O-Si or Si-O-Al, whereas the hydrophobic moiety still links with the Si atoms through Si-C covalent bonds. The Si-C covalent bonds hinder the growth of zeolite crystal in the corresponding direction. Thus the crystal defects in the zeolite are generated, and after calcination, these defects turn into mesopores.

Herein, we report the synthesis of zeolite LTA with intracrystalline mesopores by optimizing synthesis conditions, including alkalinity, synthesis mixture Si/Al molar ratio and crystallization time. We also discuss the controlling factors of mesoporous size and volume.

1 Experimental

1.1 Synthesis

The organosilanes were Phenylaminopropyl-trimethoxysilane (Y-5669, Sigma-Aldrich), *N*-(Vinylbenzyl)-2-aminoethyl-3-aminopropyltrimethoxysilane hydrochloride solution (Z-6032, 40wt% in methanol, Dow Corning), KH-613 (Nanjing Capatue Chemical Co., China), and octadecyldimethylammonium chloride (TPOAC, Sigma-Aldrich), respectively.

Y-5669

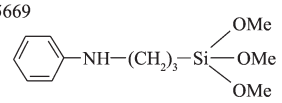

Z-6032

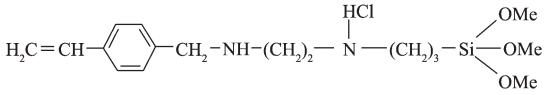

KH-613

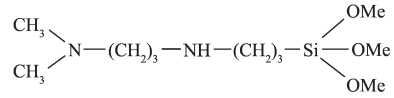

TPOAC

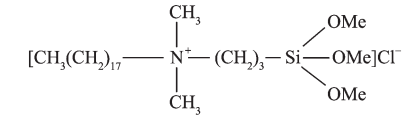

Scheme 1 Chemical structures of organosilanes in synthesis of mesoporous zeolites

1.1.1 Organic function of fumed silica

Fumed silica was organic functionalized by an organosilane with the following molar ratio: SiO_2 : $60H_2O$:*m* organosilane: $30xCH_3OH$. *m* was from 0 to 0.2. The organosilane modified fumed silica is denoted as O-SiO_2.

1.1.2 Synthesis of mesoporous zeolite LTA

Mesoporous zeolite LTA samples were prepared from a mixture with the following molar composition: xNa_2O:Al_2O_3:*y*O-SiO_2:$185H_2O$, where *x* was from 3 to 7 and *y* from 1.3 to 2.4. Sodium hydroxide was added into distilled water with stirring, O-SiO_2 and sodium aluminate solution were then added with stirring. The result mixture was stirred for 5 h at room temperature to obtain a homogeneous mixture. This mixture was heated at 363 K in a Teflon-coated stainless-steel autoclave for 2 to 20 h. Then the final samples were

washed with distilled water, filtered by centrifugation, and dried at 373 K and calcined at 823 K.

As an example, the molar composition of $5Na_2O$:Al_2O_3:$2O\text{-}SiO_2$:$180H_2O$ was used for the synthesis mixture, where the silica source was fumed silica with different Y-5669 modified degrees. The crystallization time was 20 h. The zeolitic samples are denoted as NaA-*n* for Na-type zeolite, and CaA-*n* for Ca-type zeolite (*n*=0, 1, 2, 3, 4, 5), corresponding molar ratios of organosilane Y-5669 and silica (*m*=0, 0.05, 0.07, 0.10, 0.12 , 0.16).

The used silica source was Y-5669 modified SiO_2 with a molar ratio *m*=0.16 for the synthesis mixture xNa_2O:Al_2O_3:$2O\text{-}SiO_2$:$180H_2O$, where *x*=4, 5, 6 and 7, and the crystallization time was 20 h. The samples are denoted as NaA-*x*4~NaA-*x*7 for Na-type zeolites, and CaA-*x*4~CaA-*x*7 for Ca-type zeolites.

Under the same conditions for the synthesis mixture $5Na_2O$:Al_2O_3:$yO\text{-}SiO_2$:$180H_2O$, where *y*=1.3, 1.6, 2.0 and 2.4, the samples are denoted as NaA-*y*1.3~NaA-*y*2.4 for Na-type zeolite, and CaA-*y*1.3~CaA-*y*2.4 for Ca-type zeolite.

A reference zeolite sample (denoted as zeolite NaA-0) was synthesized following the same procedure (*x*=5, *y*=2), but the silica source was pure fumed silica without organic functional group.

1.2　Ca^{2+} exchange

Ca^{2+} exchange of as-synthesized Na-zeolite samples was carried out by stirring the samples in a 0.5 mol·L^{-1} aqueous solution of $CaCl_2$ for 2 h at room temperature. This process was repeated for 3 times. Then, all Ca-zeolite samples were washed with distilled water to free from Cl^-.

1.3　Characterization

All samples were characterized by conventional techniques. XRD measurements were taken in a Shimadzu XRD-6000 using scintillation counter and Cu *Kα* radiation (*λ*=0.154 18 nm, by a CM-3121 Monochromater) operated at 40 kV and 30 mA with step size of 0.02°. The 2*θ* value was scanned in the range of 5~35° with a resolution of 5 min^{-1}. Nitrogen adsorption-desorption isotherms at 77 K were obtained in a Quantachrome NOVA 1200e. The samples were first outgassed at 613K in vacuum for 5 h. The total surface area was obtained by BET equation whereas the external surface area and micropore volume were calculated by the t-plot method. The BJH pore size distribution was derived from the adsorption branch. Field emission scanning electron microscope (SEM) images were obtained in a JEOL JSM-6700F (accelerated voltage 10 kV). FTIR spectra were recorded in a Shimadzu IRAffinity-1 Fourier Transform infrared spectrophotometer.

2　Results and discussion

2.1　Effect of organosilane

As shown in Fig.1, the XRD patterns of the samples prepared with different organosilane functionalized $O\text{-}SiO_2$ correspond to that of the highly crystalline zeolite NaA-0, which suggest that all samples are well-crystalline zeolite LTA. Compared with the pattern of the zeolite NaA-0, decreased intensity and broadened width of the diffraction peaks can be observed for the samples except NaA-613, which indicates that crystalline sizes of the samples prepared with TPOAC, Z-6032 and Y-5669 are somewhat decreased owing to use of organosilanated $O\text{-}SiO_2$. The XRD pattern of NaA-613 shows almost the same as that of zeolite NaA-0.

As shown in Fig.2, obvious difference of the sample morphologies emerges in the SEM images. The image of zeolite NaA-0 exhibits an intrinsic cubic shape of zeolite LTA with truncated edges, whereas

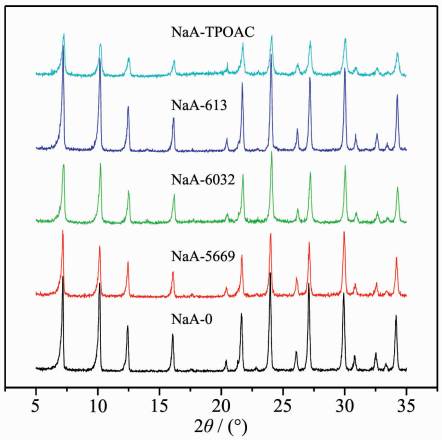

Fig.1　XRD patterns for meso-zeolite LTA synthesized with different organosilanated $O\text{-}SiO_2$ and the reference sample NaA-0

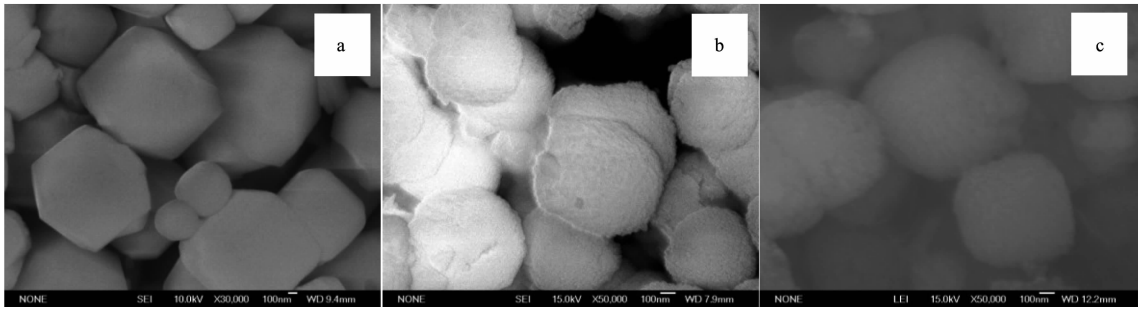

Fig.2 SEM images of the zeolite samples NaA a: NaA-0; b: NaA-5669; c: NaA-6032

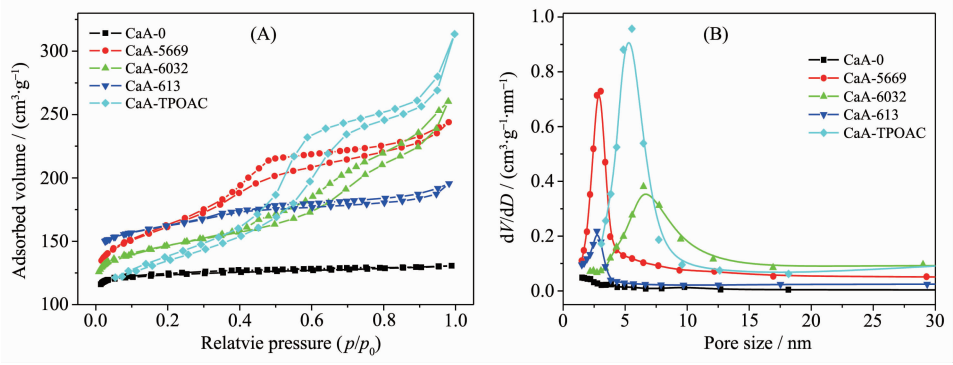

Fig.3 N_2 adsorption-desorption isotherms at 77 K (A) and BJH pore size distribution derived from the adsorption branch (B) of zeolite CaA synthesized with different organosilanated O-SiO_2

the zeolite NaA-5669 and NaA-6032 exhibit global morphology with the rugged surfaces.

Fig.3 provides the N_2 adsorption-desorption isotherms of Ca-exchanged zeolite samples at 77 K (Fig.3A) and the BJH pore size distribution derived from adsorption branch (Fig.3B). The N_2 adsorption isotherm of the zeolite CaA-0 is a traditional type Ⅰ isotherm according to the IUPAC, without obvious N_2 condensation in the pressure range of 0.2 ~0.9. In contrast, the isotherms of the other four samples prepared with the organosilane functionalized O-SiO_2 show a remarkable difference from the reference sample CaA-0. All the isotherms exhibit a strong adsorption at low relative pressure (p/p_0<0.1) corresponding to the filling of the microporous structure. However, a rather remarkable adsorption is also observed at p/p_0= 0.2~0.9, which is owing to the capillary condensation inside the mesopores, suggesting the presence of mesopores inside the zeolite crystals. This remarkable difference can be observed especially for the samples prepared using Y-5669, Z-6032 and TPOAC silanes. For the zeolites CaA-5669 and CaA-613, the obvious enhance of adsorption amount occurs at p/p_0=0.2~0.6, showing the existence of small mesopores inside the zeolite crystals. For the samples CaA-TPOAC and CaA-6032, the enhancive amounts arise at p/p_0=0.5~ 0.7 and 0.5~0.9, respectively, corresponding to relative large mesopores inside the zeolite crystals. These can be observed intuitively from the pore size distributions derived from the adsorption branch as shown in Fig. 3B. The organic moiety sizes of Y-5669 and KH-613 are about the same, being smaller than the sizes of TPOAC and Z-6032. So the size of mesopores created inside the zeolite crystals is identical for the samples of NaA-5669 and NaA-613, whereas the samples prepared using O-SiO_2 with NaA-TPOAC and NaA-6032 have larger intracrystal mesoporous diameters. The full width at half maximum (FWHM) of pore size distribution for these samples is different. For CaA-5669, CaA-613 and CaA-TPOAC, a narrower distribution of mesoporous diameters can be observed, whereas a relatively wide pore size distribution can be noticed for the sample of CaA-6032. As depicted in Fig.3B, the mesoporous diameter of the samples CaA-5669 and CaA-613 are centered at *ca.* 2.8 nm, but that of the sample CaA-TPOAC is 5.3 nm, whereas

Table 1　Pore structure parameters of zeolite samples synthesized with different organosilanes

Samples	S_{BET} / ($m^2 \cdot g^{-1}$)	S_{micro} / ($m^2 \cdot g^{-1}$)	S_{Ext} / ($m^2 \cdot g^{-1}$)	V_{micro} / ($cm^3 \cdot g^{-1}$)	V_{meso} / ($cm^3 \cdot g^{-1}$)
CaA-0	510	481	29	0.18	0.01
CaA-5669	608	248	360	0.10	0.27
CaA-6032	570	441	129	0.17	0.25
CaA-613	631	518	113	0.20	0.09
CaA-TPOAC	457	260	197	0.09	0.35

that of the sample CaA-6032 centers at *ca.* 6.5 nm with a relative wide FWHM. Therefore, the intracrystal mesopore diameter in the zeolite LTA samples is affected and modulated by using the organosilanated O-SiO_2 with different organosilanes.

The pore structure parameters of the zeolitic samples in Table 1 indicate that the mesoporous zeolite materials prepared with the organosilane functionalized O-SiO_2 present higher BET surface area, external surface area and mesoporous volume. For the sample prepared with Y-5669, the BET area, external surface area and mesoporous volume reach 608 $m^2 \cdot g^{-1}$, 360 $m^2 \cdot g^{-1}$ and 0.27 $mL \cdot g^{-1}$, respectively, while the corresponding values for sample CaA-0 are only 510 $m^2 \cdot g^{-1}$, 29 $m^2 \cdot g^{-1}$ and 0.02 $mL \cdot g^{-1}$. The data listed in Table 1 reflects also that the formation mechanism of mesopores in the samples is different from each other.

From an evaluation of the results of the samples prepared from four different organosilanes, the sample CaA-5669 is the best mesoporous zeolite LTA because of its higher full surface area and external surface area from the mesopores, as well as its narrower pore size distribution inside the zeolite crystals.

2.2　Influence of synthesis conditions

It is remarkable that the zeolite sample CaA-5669 prepared with functionalized O-SiO_2 by organosilane Y-5669 shows a maximum mesoporous amount and a narrow pore size distribution. We have found that synthesis conditions have important influences on the mesostructured zeolite LTA too.

2.2.1　$n_{Na_2O}/n_{Al_2O_3}$ ratio

As shown in Fig.4, all samples are high crystalline zeolite LTA and their crystallinity degrees are almost identical, though with the different $n_{Na_2O}/n_{Al_2O_3}$ ratios when x varies from 4 to 7.

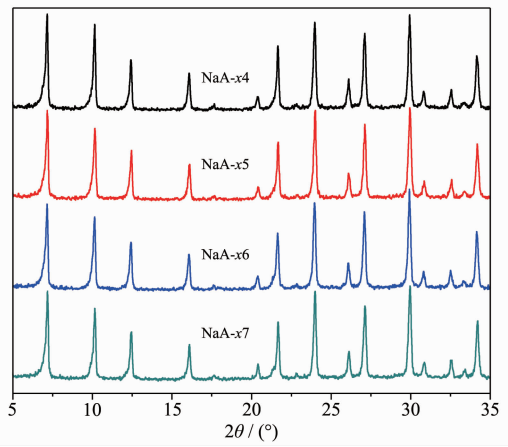

Fig.4　XRD patterns for meso-zeolite NaA synthesized by different basicities

The nitrogen adsorption-desorption isotherms in Fig.5A show typical mesoporous characteristics of the samples prepared in the range of $n_{Na_2O}/n_{Al_2O_3}$ ratios studied. The samples CaA-x5, CaA-x6 and CaA-x7 exhibit higher nitrogen adsorption volumes than sample CaA-x4, while the pore size distributions remain the same outline for all samples and center at 2.8~3 nm with a narrow FWHM shown in Fig.5B. The structure parameters in Table 2 derived from the nitrogen adsorption-desorption isotherms confirm that all synthesized samples process high mesoporous volume compared with the reference zeolite sample CaA-0 with only low mesoporous volume of 0.01 $cm^3 \cdot g^{-1}$.

2.2.2　SiO_2/Al_2O_3 ratio

As shown the XRD patterns in Fig.6, all samples are assigned to high crystalline zeolite LTA. However, as increasing SiO_2/Al_2O_3 molar ratio of the synthesis mixture reaches to larger than 2.4, the zeolite X phase is produced, and as decreasing the SiO_2/Al_2O_3 molar ratio to smaller than 1.3, the crystallinity degree of the sample begins to reduce.

Fig.7 shows the nitrogen adsorption-desorption isotherms of the samples and the BJH pore size

Table 2 Pore structure parameters of meso-zeolite samples synthesized by different nN_2O/nAl_2O_3

Samples	S_{BET} / ($m^2 \cdot g^{-1}$)	S_{Ext} / ($m^2 \cdot g^{-1}$)	V_{micro} / ($cm^3 \cdot g^{-1}$)	V_{meso} / ($cm^3 \cdot g^{-1}$)
CaA-*x*4	587	312	0.11	0.19
CaA-*x*5	608	360	0.10	0.27
CaA-*x*6	619	298	0.13	0.22
CaA-*x*7	599	289	0.12	0.21

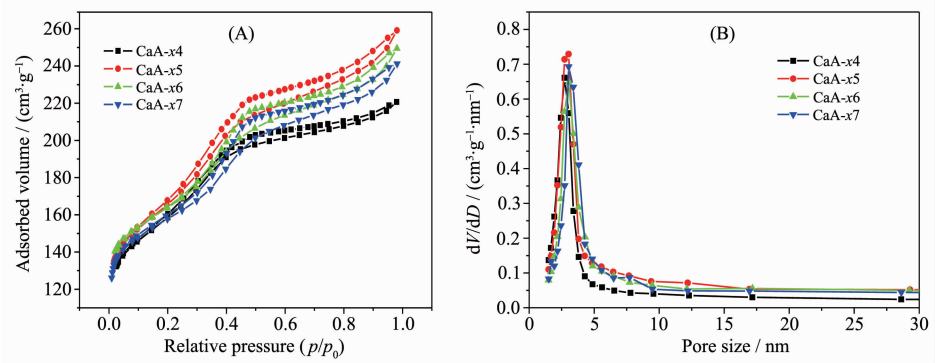

Fig.5 N_2 adsorption-desorption isotherms at 77 K (A) and BJH pore size distribution derived from the adsorption branch (B) of meso-zeolite NaA synthesized by different basicities

distributions. The four isotherms own all typical mesoporous characteristics as illustrated in Fig.6.

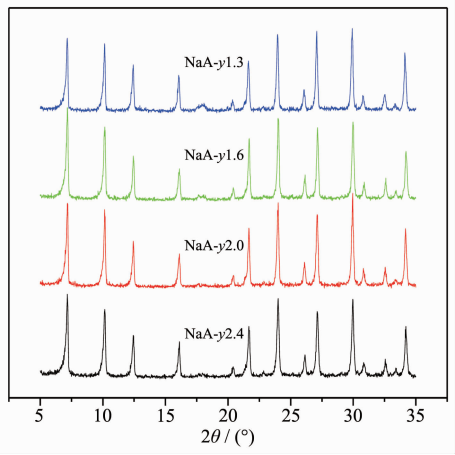

Fig.6 XRD patterns for meso-zeolite NaA synthesized with different Si/Al molar ratios

Zeolite CaA-*y*2.0 and CaA-*y*1.6 have higher nitrogen adsorption volume than other two samples. The pore size distribution shown in Fig.7B indicates that the narrow pore size distribution of all samples is centered at 2.8~3.0 nm. The corresponding structure parameters of the samples are included in Table 3.

2.2.3 Crystallization time

The crystalline process of zeolite presents a distinct S-type curve. As depicted in Fig.8, no zeolite crystalline phase is detected after one hour′ s hydrothermal crystallization, while the zeolite LTA crystal appears after 2 h, and the crystallinity degree increases with time. After 5 hours′ hydrothermal crystallization, the crystallinity degree of the samples is kept constant and the stable state could be held to

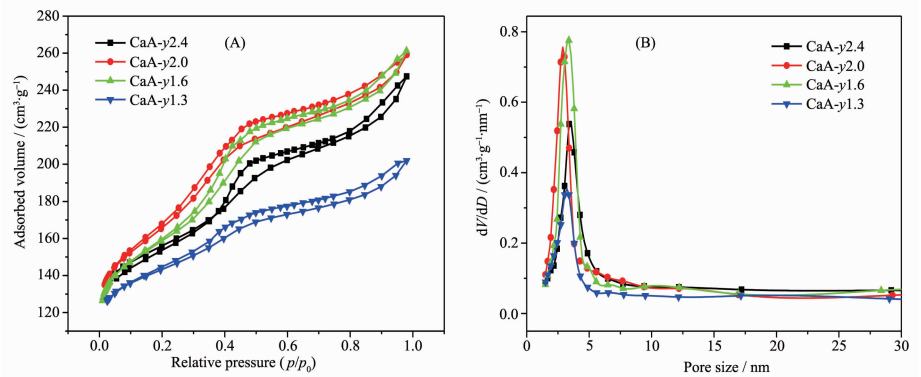

Fig.7 N_2 adsorption-desorption isotherms at 77 K (A) and BJH pore size distribution derived from he adsorption branch (B) of meso-zeolite CaA synthesized with different Si/Al molar ratios

Table 3　Pore structure parameter of meso-zeolite CaA synthesized with different $nSiO_2/nAl_2O_3$

Samples	S_{BET} / ($m^2 \cdot g^{-1}$)	S_{Ext} / ($m^2 \cdot g^{-1}$)	V_{micro} / ($cm^3 \cdot g^{-1}$)	V_{meso} / ($cm^3 \cdot g^{-1}$)
CaA-*y*2.4	590	242	0.14	0.21
CaA-*y*2.0	608	360	0.10	0.27
CaA-*y*1.6	587	345	0.10	0.25
CaA-*y*1.3	546	187	0.14	0.15

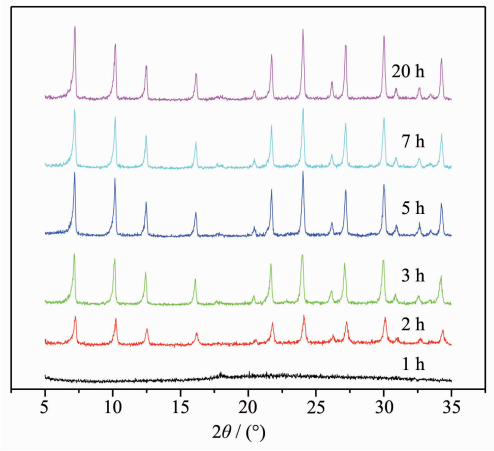

Fig.8　XRD patterns for meso-zeolite NaA synthesized with different crystallization times

more than 20 h, showing the structural stability of the mesoporous zeolite LTA prepared by the organosilanation silica.

2.3　Formation of mesoporous structure

To clarify the formation of the mesoporous structure in zeolite crystals, the crystallization of the samples was tracked by IR spectroscopy, XRD and SEM. The corresponding XRD pattern is shown in Fig.8. FTIR spectra of as-synthesized zeolitic samples are shown in Fig.9. After one hour′s hydrothermal crystallization, a clear shoulder in the region of

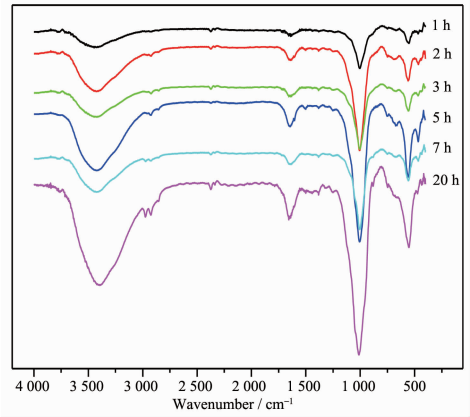

Fig.9　FTIR spectra of as-synthesized LTA samples with different crystallization times

zeolitic framework vibrations (500~1 000 cm^{-1}) can be seen, revealing signs of zeolite, though XRD patterns display only an amorphous framework structure. After two hours′ hydrothermal crystallization, X-ray diffraction characteristics of zeolite LTA appear as shown clearly in Fig.8. The results indicate that zeolitic seeds have formed within one hour and grown to long range order within two hours. The vibration wavenumbers at about 2 975 cm^{-1}, 2 930 cm^{-1}, 2 853 cm^{-1}, 1 600 cm^{-1}, 1 500 cm^{-1} and 1 450 cm^{-1} confirm that the organosilane is grafted on the external surface of zeolite LTA crystals successfully.

The SEM images of the zeolitic samples at different hydrothermal crystallization times are presented in Fig.10. For hydrothermal crystallization after 1 h, only amorphous particles are found, which corresponds to X-ray amorphous results. Though large numbers of uniform spherical particles about 500~700 nm appear in the sample, some amorphous components still exist after 2 hours′ crystallization. With the increase of the crystallization time, the crystallinity of the sample increases but the diameters of the spherical particles remain unchanged. The final products show typical spherical morphology with the rugged surface (see Fig.2b too).

Surface areas and pore volumes of the as-synthesized zeolitic samples are determined using nitrogen adsorption-desorption isotherms at 77 K (Fig. 11 and Table 4). As shown in Fig.11A, the mesoporous structure in the zeolitic sample begins to be constructed during the earliest crystallization. The mesoporous diameters in the zeolitic samples contract gradually from 3.8 nm to 2.8 nm with increasing crystallization time (Fig.11B). Incidentally, full surface area and external surface area increase (Table 4). The results are from the formation and regulation (high crytallinity and narrow pore distribution) of the intracrystalline

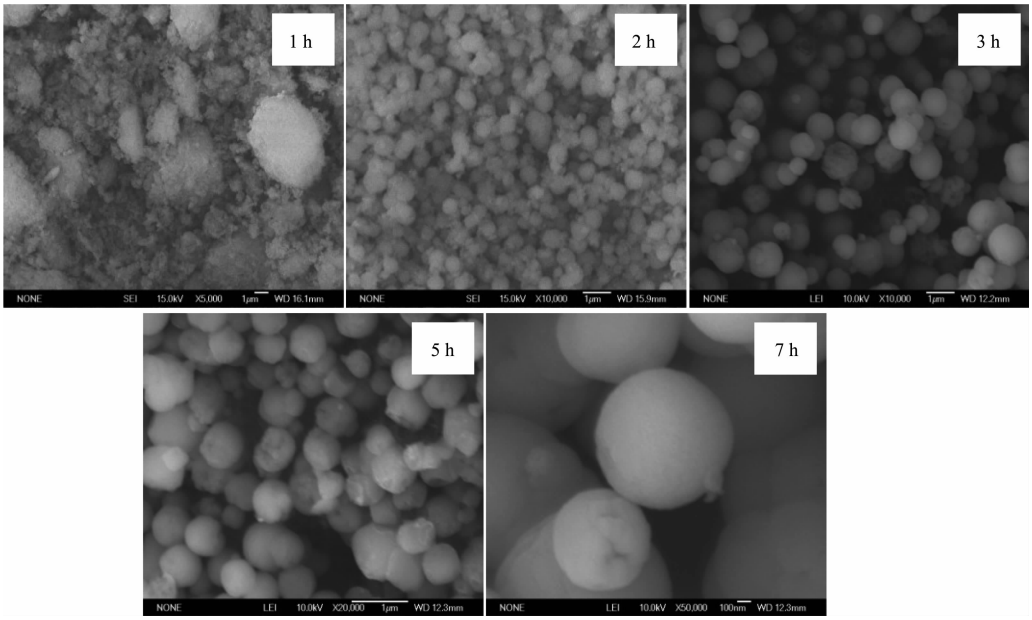

Fig.10 SEM images for meso-zeolite NaA synthesized with different crystallization time

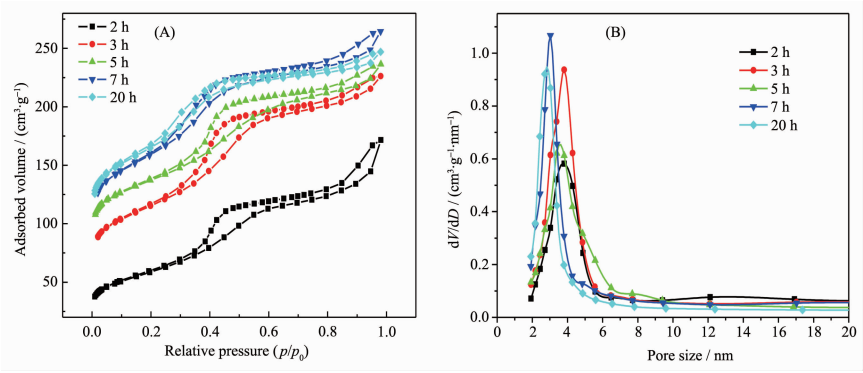

Fig.11 N_2 adsorption-desorption isotherms at 77 K (A) and BJH pore size distribution derived from the adsorption branch (B) of meso-zeolite CaA synthesized with different crystallization times

Table 4 Pore structure parameters of meso-zeolite samples synthesized with different crystallization times

Sample	S_{BET} / ($m^2 \cdot g^{-1}$)	S_{Ext} / ($m^2 \cdot g^{-1}$)	V_{micro} / ($cm^3 \cdot g^{-1}$)	V_{meso} / ($cm^3 \cdot g^{-1}$)	D_{meso} / nm
CaA-1 h	—	—	—	—	—
CaA-2 h	192	192	0	0.20	3.8
CaA-3 h	415	277	0.06	0.20	3.8
CaA-5 h	507	249	0.11	0.25	3.6
CaA-7 h	578	331	0.10	0.24	3.0
CaA-20 h	608	360	0.10	0.27	2.8

mesoporous structure in the zeolitic crystals.

It is clear that the construction of intracrystalline pores begins from the earliest stage. The organofunctioned and the unorganofunctioned silica as elemental units autonomically congregate spherules to be crystallized during the hydrothermal reaction. Growth of crystals and Si-C bond-blocking arise at one time, resulting in the formation of microporous zeolite and mesoporous structure in the small beads. Finally, the centripetal force of crystalline growth and the repelling force of bond-blocking keep a balance to create a spherical mesostructured zeolite LTA.

2.4 Influence of organic function degree

In the formation of the mesoporous structure, how is the influence of organofunctioned degree of silica on the mesostructured zeolite LTA? The fumed silica

with different Y-5669 modified degree was used in the mesoporous materials. As illustrated in Fig.12, XRD patterns of the samples prepared with different organic function degrees agree well with highly crystalline zeolite NaA-0. They have the same crystalline size and are not aggregated nanocrystals. During the hydrothermal crystallization process, more hydrophobic moiety hinders the growth of zeolite crystals in that position, thus more mesopores are created. This confirms that the synthesis method demonstrated is a practical way for hydrothermal synthesis of zeolite LTA with tunable intracrystalline mesopores.

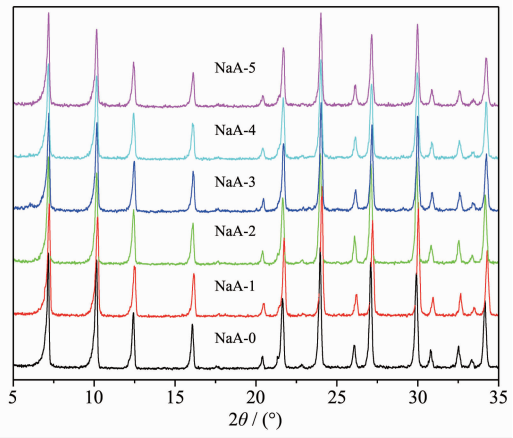

Fig.12　XRD patterns for meso-zeolite NaA synthesized with different organic function degrees

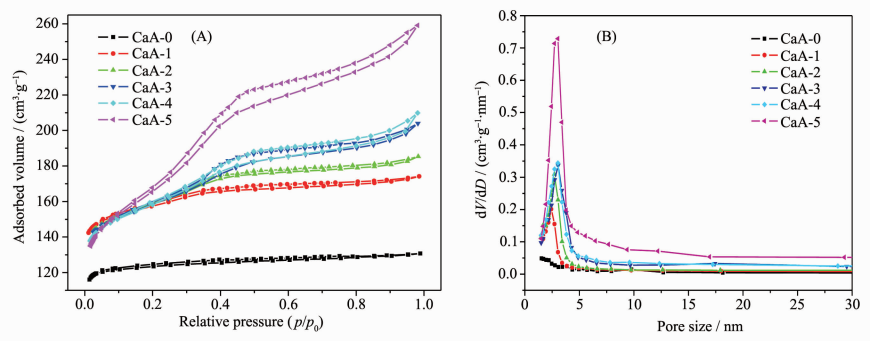

Fig.13　N_2 adsorption-desorption isotherms at 77 K (A) and BJH pore size distribution derived from the adsorption branch (B) of meso-zeolite CaA synthesized with different organic function degrees

3　Conclusions

In conclusion, the zeolite LTA with intracrystalline mesopores was synthesized using organic functionalized SiO_2 as silica source. The synthesis mixture with $n_{Na_2O}/n_{Al_2O_3}$ of 5~6, $n_{Na_2O}/n_{Al_2O_3}$ of 1.6~2.0 and the crystallization time longer than 7 h is the best synthesis condition for producing mesoporous zeolite LTA. Four different organosilanes are selected and Y-5669 is the best one to create intracrystalline mesopores in zeolite LTA crystal. The mesoporous sizes can be modulated by selecting different kinds of organosilanes. Within a certain range, the external surface area and mesoporous volume increase along with the increase of the organic function degree of the silica source. This conforms that the synthesis method in this work is a suitable way for hydrothermal synthesis of zeolite LTA with tunable intracrystalline mesopores.

Acknowledgment: This work was financially supported by the National Nature Science Foundation of China (Grant No. 50872087).

References:

[1] Corma A. *Chem. Rev.*, **1997**,**97**:2373-2420
[2] Meng X, Nawaz F, Xiao F S. *Nano Today*, **2009**,**4**:292-301
[3] Tao Y, Kanoh H, Kaneko K, et al. *Chem. Rev.*, **2006**,**106**:896-910
[4] Pérez-Ramírez J, Christensen C H, Egeblad K, et al. *Chem. Soc. Rev.*, **2008**,**37**:2530-2542
[5] Kresten E, Christina H C, Marina K, et al. *Chem. Mater.*, **2008**,**20**:946-960
[6] Sander Van D, Andries H J, Johannes H B, et al. *Catal. Rev.*, **2003**,**45**:297-319
[7] Lopez-Orozco S, Inayat A, Schwab A, et al. *Adv. Mater.*, **2011**,**23**:2602-2615
[8] Le H, Zhou J, Shi J, *Chem. Commun.*, **2011**,**47**:10536-10547
[9] Pérez-Ramírez J, Abello S, Bonilla A, et al. *Adv. Funct. Mater.*, **2009**,**19**:164-172

[10]Corma A, Fornes V, Pergher S B, et al. *Nature*, **1998**,**396**:353-356

[11]Groen J C, Moulijn J A, Pérez-Ramírez J. *J. Mater. Chem.*, **2006**,**16**:2121-2131

[12]Groen J C, Abello S, Villaescusa L A, et al. *Micropor. Mesopor. Mat.*, **2008**,**114**:93-102

[13]Danny V, Pérez-Ramírez J. *Chem.-Eur. J.*, **2011**,**17**:1137-1147

[14]Groen J C, Hamminga G M, Moulijn J A, et al. *Phys. Chem. Chem. Phys.*, **2007**,**9**:4822-4830

[15]Serrano D P, Aguado J, Escola J M, et al. *Chem. Mater.*, **2006**,**18**:2462-2464

[16]Larsen S C. *J. Phys. Chem. C*, **2007**,**111**:18464-18474

[17]Rakoczy R A, Traa Y. *Micropor. Mesopor. Mat.*, **2003**,**60**:69-78

[18]Lubomira T, Valtchev V P. *Chem. Mater.*, **2005**,**17**:2494-2513

[19]Jacobsen C J H, Madsen C, Houzvicka J, et al. *J. Am. Chem. Soc.*, **2000**,**122**:7116-7117

[20]Schmidt I, Boisen A, Gustavsson E, et al. *Chem. Mater.*, **2001**,**13**(12):4416-4418

[21]Zhu H, Liu Z, Wang Y, et al. *Chem. Mater.*, **2008**,**20**:1134-1139

[22]Tao Y, Kanoh H, Kaneko K. *J. Phys. Chem. B*, **2003**,**107**:10974-10976

[23]Choi M, Cho H S, Srivastava R, et al. *Nat. Mater.*, **2006**,**5**:718-723

[24]Cho K, Cho H S, Menorval De L C, et al. *Chem. Mater.*, **2009**,**21**:5664-5673

[25]Xue Z, Ma J, Hao W, et al. *J. Mater. Chem.*, **2012**,**22**:2532-2538

[26]Xue Z, Ma J, Zhang T, et al. *Mater. Lett.*, **2012**,**68**:1-3

[27]Xue Z, Zhang T, Ma J, et al. *Micropor. Mesopor. Mat.*, **2012**,**151**:271-276

[28]Katsuyuki T, Christopher W J, Davis M E. *Micropor. Mesopor. Mat.*, **1999**,**29**:339-349

[29]Christopher W J, Katsuyuki T, Davis M E. *Micropor. Mesopor. Mat.*, **1999**,**33**:223-240